PNAS
www.pnas.org

Main Manuscript for

Significant Zr isotope variations in single zircon grains recording magma evolution history

Jing-Liang Guo [a,b,1], Zaicong Wang [a,1], Wen Zhang [a], Frédéric Moynier [a,c], Dandan Cui [a], Zhaochu Hu [a], Mihai N Ducea [b,d]

[a] State Key Laboratory of Geological Processes and Mineral Resources, School of Earth Sciences, China University of Geosciences, Wuhan 430074, China

[b] Department of Geosciences, University of Arizona, Tucson, AZ 85718, United States

[c] Institut de Physique du Globe de Paris, Université de Paris, CNRS, 1 rue Jussieu, 75238 Paris cedex 05, France

[d] Faculty of Geology and Geophysics, University of Bucharest, Bucharest 010041, Romania

[1] Jing-Liang Guo

Email: jl.guo@cug.edu.cn

ORCID: 0000-0003-4890-4028

[1] Zaicong Wang

Email: zaicongwang@cug.edu.cn

ORCID: 0000-0002-3584-1673

Classification

Physical Science – Earth, Atmospheric, and Planetary Sciences

Keywords

Zr isotopes; Zircon; Magma temperature; Laser ablation MC-ICP-MS; Crustal differentiation

Author Contributions

J.-L.G., Z.W. and Z.H. designed research; J.-L.G., Z.W. and F.M. performed research; J-L.G., D.C. and W.Z. analyzed data; J.-L.G., Z.W., W.Z. and F.M. contributed to the data interpretation and manuscript writing. M.N.D. contributed to the igneous aspect of the manuscript and manuscript revision.

Competing interests

The authors declare no competing interests.

This PDF file includes:

Main Text
Figures 1 to 5

Abstract

Zircons widely occur in magmatic rocks and often display internal zonation finely recording the magmatic history. Here, we presented in-situ high-precision (2SD <0.15‰ for δ^{94}Zr) and high-spatial-resolution (20 μm) stable Zr isotope compositions of magmatic zircons in a suite of calc-alkaline plutonic rocks from the juvenile part of the Gangdese arc, southern Tibet. These zircon grains are internally zoned with Zr isotopically light cores and increasingly heavier rims. Our data suggest the preferential incorporation of lighter Zr isotopes in zircon from the melt, which would drive the residual melt to heavier values. The Rayleigh distillation model can well explain the observed internal zoning in single zircon grains, and the best-fit models gave average zircon–melt fractionation factors for each sample ranging from 0.99955 to 0.99988. The average fractionation factors are positively correlated with the median Ti-in-zircon temperatures, indicating a strong temperature dependence of Zr isotope fractionation. The results demonstrate that in-situ Zr isotope analyses would be another powerful contribution to the geochemical toolbox related to zircon. The findings of this study solve the fundamental issue on how zircon fractionates Zr isotopes in calc-alkaline magmas, the major type of magmas that led to forming continental crust over time. The results also show the great potential of stable Zr isotopes in tracing magmatic thermal and chemical evolution and thus continental crustal differentiation.

Significance Statement

Zircon, a common and resistant accessory mineral in crustal rocks, records plentiful and critical information on the Earth's history. The isotopes of its major component Zr could be another powerful, but unexplored tracer. We apply high-precision, high-spatial-resolution, in-situ laser ablation Zr isotope measurements of magmatic zircons in continental arc plutonic rocks. Single zircon grains show impressive internal zoning with lighter Zr isotopes in the core but heavier toward the rim, solving a fundamental but controversial issue on how zircon fractionates Zr isotope in evolving magmas. Our results also reveal a strong temperature dependence of Zr isotopic fractionation. The Zr isotope is thus very promising in deciphering magmatic differentiation history and the formation and evolution of continental crust through time.

Main Text

Introduction

Zircon ($ZrSiO_4$) is one of the most important accessory minerals in rocks. It occurs in a large variety of lithologies and is generated primarily in intermediate to felsic igneous rocks (1, 2). Its trace element (e.g., Ti and REE) and isotopic (e.g., U–Pb, Lu–Hf, Si, and O) abundances have provided major information on the absolute timing, petrochronologic conditions, and tectonic backgrounds of important geological events along the Earth's history (3–8). They are especially important for deciphering the growth and reworking history of the continental crust (9), the early differentiation of the Earth (4, 10), and the styles of plate tectonics through time (11, 12).

Magmatic zircons crystallize early in evolved calc-alkaline magmas (1). They are relatively insoluble in crustal melts and resistant to chemical and physical breakdown. The diffusion of major and trace elements is also sluggish (13). These characteristics allow zircon to preserve elemental and isotopic zoning, as well as several generations of geochemical information within a single grain (2, 13). Compared to bulk analyses, in-situ analytical methods could extract more detailed thermal and chemical information from intragrain chemical zoning (14, 15). Since zircon has significantly higher Zr concentration (~48 wt.% as a major element) than rock-forming minerals (0 to 10s ppm) (16), the Zr content of magmas should be primarily controlled by zircon after its saturation. Given that Zr is incompatible during mantle melting, and that it has long been used to monitor magmatic differentiation processes of the silicate Earth (17, 18), the Zr isotopes of zircon may also record related information.

Recent developments of bulk and in-situ analytical methods have permitted studies on mass-dependent Zr isotope fractionation in terrestrial samples, including zircons (15, 19–24). They show the great potential of Zr isotope in tracing magmatic processes. However, available data have been rather limited, and resulted in the very controversial interpretation (21, 22) such as for

fractionation factor α (whether greater or smaller than 1). The α is defined as $(^{94}Zr/^{90}Zr)_{zircon}/(^{94}Zr/^{90}Zr)_{melt}$, which depicts how Zr isotopes partition into the crystallizing zircon and surrounding melt and is thus fundamental to understand magmatic Zr isotope evolution. Inglis et al. (21) studied a highly differentiated magmatic suite from the Hekla volcano in Iceland, and suggested an α of 0.9995, given the increasing $\delta^{94}Zr$ (up to 0.527‰; $\delta^{94}Zr$ is the permil deviation of $^{94}Zr/^{90}Zr$ from the IPGP-Zr standard) along with decreasing Zr contents in highly evolved samples (SiO_2 >65 wt.%). It implies that zircon favors light Zr isotopes from the melt, consistent with theoretical predictions based on the Zr-coordination difference between zircon and the melt (21). On the other hand, zircon crystals extracted from FC1 gabbroic anorthosite (Duluth Complex, NE Minnesota) show extremely large Zr isotope variations (~5‰), revealed by both in-situ (15) and bulk measurements (22). The majority of bulk-zircon values are heavier than the bulk rock, and an α of 1.00106 was suggested accordingly (22). While these studies reached opposite conclusions, they both suggested that zircon crystallization would fractionate the Zr isotope composition of the melt. This effect might be recorded in the growth zoning of single zircon grains.

The internal growth zoning in magmatic zircons is common (2), and once formed, it could preserve information on the subtle and transient magmatic differentiation due to the negligible diffusion of tetravalent cations (25). Thus, high-spatial-resolution in-situ analyses of internally zoned zircon grains may provide key insights into magma differentiation. Here we apply high-precision laser ablation (LA) MC-ICP-MS and report in-situ Zr isotope compositions of magmatic zircons from mafic to intermediate plutonic rocks, which represent the juvenile part of the Gangdese arc in southern Tibet (26, 27). The results reveal large internal Zr isotope variations in single grains, showing unambiguously the preference of light Zr isotope by zircons and set the base for wide future applications. This study further indicates the control of magmatic temperature on zircon–melt Zr isotope fractionation, suggesting its potential in depicting magmatic thermal and chemical evolution.

Mafic–intermediate plutonic rocks and zircons from the Gangdese arc, southern Tibet

The Gangdese arc in southern Tibet was produced by the northward subduction of the Neo-Tethyan oceanic lithosphere during the Mesozoic; this arc later witnessed the India–Asia collision during the Cenozoic (26, 28). Large volumes of Mesozoic plutonic rocks outcropped along the eastern segment of the Gangdese arc. These rocks typically show depleted mantle-like isotopic features, indicating significant juvenile crustal growth during this period (26). The studied samples belong to a suite of mafic–intermediate plutonic rocks collected from the Quxu batholith in the eastern Gangdese arc, including hornblende gabbros, tonalites, and biotite-rich microgranular enclaves hosted by the tonalites (Fig. 1 and *SI Appendix*, Tables S1). These samples represent the juvenile part of Gangdese arc crust formed mainly by fractional crystallization of arc magmas

(27). Zirconium isotopes of the zircons may have recorded the differentiation of those calc-alkaline arc plutonic rocks. Here we analyzed their U–Pb ages, major and trace element compositions, as well s Zr isotope compositions.

Zircons are rare in hornblende gabbros but are common in tonalites and biotite-rich enclaves. Most extracted grains are ~100–300 μm in length with euhedral shapes. They vary in size and internal structure among different rock types (Fig. 2). Zircons from the hornblende gabbros are generally smaller and have linear, sector, or wide-banded oscillatory zoning (Fig. 2 *A–F*). In contrast, zircons from the tonalites and the biotite-rich enclave are larger and show dominantly oscillatory zoning with thin bands (Fig. 2 *G–J*). These features, together with high Th/U ratios (0.4–2.9) (*SI Appendix*, Table S2), indicate a magmatic origin (2). No systematic U–Pb age difference was found between the core and the rim. The emplacement ages of all samples range from ~90 Ma to ~96 Ma (*SI Appendix*, Fig. S1 and Table S2), which are consistent with the magmatic flare-up (100–85 Ma) of regional arc magmatism (26). Bulk-rock geochemical features further suggest these samples as part of the juvenile crust formed during the Late Cretaceous (*SI Appendix*, Fig. S2 and Table S3).

The Zr isotope compositions of magmatic zircons were analyzed by femtosecond LA-MC-ICP-MS using a small spot size of 20 μm, which assured the high spatial resolution and high precision (*SI Appendix*, Table S4). Isotope ratios were calibrated against zircon standard GJ-1 or Penglai, which are homogeneous in Zr isotope compositions shown by Zhang et al. (15). GJ-1 is a gem-quality megacryst zircon from Sri Lanka that has been widely used for U–Pb and Hf isotope analysis (29). The Penglai zircon is megacrysts (up to several millimeters in length) from Quaternary potassic basalts in south China used for O and Hf isotope analysis (30). Both were shown homogeneous in Zr isotope compositions (15). In order to directly compare our zircon data with previous bulk analyses, the $^{94}Zr/^{90}Zr$ ratios were further expressed as the permil deviation from solution standard IPGP-Zr (Plasma-Cal^{TM} standard solution; Lot: 5131203028). This standard has been used as a reference standard in most studies reporting Zr isotopic compositions and was recently cross-calibrated with different geological reference materials (15, 20, 21, 23). The within-run and long-term external precision for $\delta^{94}Zr$ in this study are better than 0.10‰ (2SE) and 0.15‰ (2SD), respectively. The $\delta^{94}Zr$ values of all analyzed zircons range from −0.86‰ to 0.41‰, with an average of −0.04±0.39‰ (2SD, n=237). The overall range (1.27‰) is larger than recently reported bulk rocks (0.582‰) (21), but smaller than that (~5‰) observed in zircon and baddeleyite crystals from anorthosite FC1 (15, 22).

Most zircon grains in this study show well-developed internal isotope zoning (Figs. 2 and 3). The intragrain variations can be as significant as 0.74‰, with an average of 0.31±0.38‰ (2SD, n=38) (*SI Appendix*, Table S4). The isotope profiles are characterized by low $\delta^{94}Zr$ in the core and

elevated values toward the rim (Figs. 2 and 3). The average δ^{94}Zr value of zircon core for each sample shows a negative correlation with the relative core–rim difference ($\Delta_{Rim-Core}$) (*SI Appendix*, Table S1). A few zircon grains show complex zoning patterns with elevated or reduced δ^{94}Zr values at the mantle relative to the core (e.g., Figs. 2 *G*, *J* and *L*). Some of them show truncation surfaces in the core (e.g., Figs. 2*L*), indicating a possible antecrystic origin (inherited from previous magmatic pulses) given the indistinguishable ages (31).

Major and trace element profiles were also obtained along the Zr isotope profiles (*SI Appendix*, Table S5). The Zr/Hf profiles generally decrease from core to rim, opposite to δ^{94}Zr (Fig. 2). This trend is clearer for zircons in samples with lower magmatic temperatures, and the slopes of δ^{94}Zr vs. Zr/Hf for single zircon grains become steeper from hornblende gabbros to tonalites and the biotite-rich enclave (*SI Appendix*, Fig. S5). The Zr/Hf ratio of zircon has been used as an indicator for magmatic differentiation; zircons from more evolved melts tend to have lower Zr/Hf ratios (32). The broadly negative correlation between δ^{94}Zr values and Zr/Hf ratios implies that the Zr isotope variations in zircon also records magmatic differentiation related to zircon crystallization.

The crystallization temperature of zircon was estimated using the Ti-in-zircon thermometer (34) (*SI Appendix*, Tables S2 and S5). This thermometer requires inputs of zircon Ti concentrations, bulk-rock SiO_2 and TiO_2 activities, and the pressure. The activities have a critical impact on the estimated temperatures (34), which were calculated using the thermodynamic software Perple_X (35) except for the biotite-rich enclave. This sample has quartz and rutile (inclusions in biotite), and thus the activities of SiO_2 and TiO_2 were both assigned to 1. The obtained temperatures were further corrected to 0.4 GPa (corresponding to a temperature increase of 30 °C) (33). The studied samples show systematic differences in the median Ti-in-zircon temperature: 743–831 °C for hornblende gabbros, 726–742 °C for tonalites, and 689 °C for the biotite-rich enclave (*SI Appendix*, Tables S1). The temperature differences in different samples are consistent with the corresponding lithology and petrographic textures (*SI Appendix*).

Significance of internal Zr isotope zoning in single zircon grains

The most significant finding in this study is the large internal Zr isotope zoning (up to 0.74‰) in single zircon grains from the studied arc plutonic rocks (Figs. 2 and 3). Chemical zoning in minerals could be induced by growth or subsequent diffusion. The diffusivity of Zr in zircon was inferred from its geochemical twin Hf, which is almost immobile in zircon even at temperatures of 900–1000 °C (25). Therefore, the Zr isotope zoning in zircon reflects most likely growth zoning, which may record the change of melt composition during magma differentiation.

Isotope profiles in these zircon grains are characterized by light cores and gradually heavier rims (Fig. 2). Most δ^{94}Zr values of the zircon cores (so does the average value of all analyses) are

lower than that of the primitive mantle (0.048.0 ± 0.032‰) (21). Such zoning patterns indicate the preferential incorporation of light Zr isotopes into zircon (i.e., α <1). Our finding is consistent with the first-order theoretical prediction where higher coordination-number lattices will be enriched in lighter isotope, since in zircons, Zr has 8-fold coordination (36) while in the melts it is generally found with 6-fold coordination (37, 38). This is also consistent with the α of 0.9995 inferred from bulk analyses of Hekla volcanic rocks, where rhyolites (SiO_2 >65 wt.%) show elevated $\delta^{94}Zr$ values with reduced Zr contents (21). It is, however, different from the α of 1.00106 suggested from FC1 zircons in the Duluth anorthosite (15, 22). The FC1 zircons exhibit a much larger $\delta^{94}Zr$ range of ~5‰ (15, 22) than observed in megacryst zircons (<0.3‰) (15, 24) or fine- to medium-grained zircons in this study (1.27‰). The majority of them are isotopically heavier than the bulk rock by ~0.3‰, resulting in α >1 (22). However the large range in FC1 was mainly caused by two low values (−2.530‰ and −4.278‰) in zircon fragments that were not treated by chemical abrasion (a method to selectively remove domains with high accumulated radiation damage) (22). If they were excluded, the range would drop to ~1.8‰ (vs. 1.27‰ in this study). One anomalously low value of −3.44‰ also exists in in-situ data, in contrast to the rest ranging from −0.84‰ to 1.49‰ (15). Radiation damage and later hydrothermal alteration were actually documented in anorthosite zircon AS3 from another outcrop in the Duluth Complex, resulting in depleted ZrO_2 and SiO_2 contents, discordant U–Pb ages, and enriched non-formula elements in metamict domains (39). Slight age discordance has also been reported for FC1 zircons (40). It is unclear whether metamictization (and later hydrothermal alteration) or different bonding environments of mafic magmas have influenced the Zr isotope composition of FC1 zircons and the bulk rock. More work is needed to answer this question.

The internal zoning in zircon can provide more direct evidence and avoid some of the potential problems faced by bulk analyses (15, 24). The observed isotope profiles can be modeled by Rayleigh distillation (Fig. 2 and *SI Appendix*, Text S6). This model assumes (1) equilibrium at the zircon–melt interface and (2) the melt is homogeneous, but once zircon is crystallized, it is considered to be isolated from the system. Assuming zircon crystallization as the only controlling factor on Zr isotope fractionation, the composition of crystallizing zircon and the residual melt (Fig. 4*A*) can be modeled using the following equations:

$$\delta^{94}Zr_{zircon} = (\delta^{94}Zr_{melt,\,0} + 1000)\,\alpha\,F^{(\alpha-1)} - 1000 \qquad (1)$$

$$\delta^{94}Zr_{melt} = (\delta^{94}Zr_{melt,\,0} + 1000)\,F^{(\alpha-1)} - 1000 \qquad (2)$$

Where $\delta^{94}Zr_{melt,\,0}$ is the initial melt isotopic composition, α is the zircon–melt isotopic fractionation factor, and F stands for the fraction of Zr content remaining in the melt. If α <1, the crystallizing zircon is isotopically lighter than the surrounding melt; while zircon grows, the melt would evolve to heavier values, and so does the lately formed zircon rims (Fig. 4*A*). The Zr isotope profile in

zircon can be further modeled by assuming sphere shapes for both zircons and the melt cell (24, 41). The radius of zircon grain would be proportional to the cubic root of 1−F (i.e., the fraction of Zr consumed by zircon) (Fig. 2 and *SI Appendix*). More complex situations can be modeled by using a recently published MATLAB routine dealing with zircon dissolution and crystallization in complex magmatic systems (41).

The fractionation factor controls not only the δ^{94}Zr difference between the crystallizing zircon and the surrounding melt, but also the shape of isotope profile (the closer the α is to 1, the flatter the profile is) (Figs. 2). Both factors were considered to determine the best-fit model, from which α can be estimated (Fig. 2). In our modeling, we avoided zircon cores that are inherited in origin. Different initial melt compositions $\delta^{94}Zr_{melt,\,0}$ (0.05‰, 0.15‰, and 0.25‰) were tested. The value of 0.05‰ is preferred unless higher values provide better fitting curves for the observed isotope profiles, especially for those with overall heavy isotope compositions (Fig. 2 and *SI Appendix*, Table S6).

The assumption of a homogeneous melt in the Rayleigh distillation model may seem to be problematic for Zr, because its diffusivity (D) is low in the melt (42, 43) and kinetic isotope fractionation may take place in the diffusive boundary melt layer near zircon (44). Since light isotopes diffuse faster, they may lead to the observed isotopically light cores of zircon. However, the growth rate (R) of zircon is normally low (45, 46), which may reasonably result in R/D ratios <0.01 cm^{-1} and significant kinetic isotope fractionation is not expected unless R/D is much higher (44). Nevertheless, zircon growth rates and Zr diffusivities in the melt are not constant. If kinetic isotope effect was in control, the produced isotope profile in single zircon grain would possibly have a “W” shape as shown for trace elements based on a diffusion-controlled crystal growth model (44), being characterized by an isotopically heavy core, a light mantle, and a heavy rim (given a finite melt cell). The estimated α for zircons with W-shaped isotope profiles could be underestimated. However, zircon δ^{94}Zr profiles in this study mostly exhibit simple U shapes, and only a few have W shapes (Fig. 2 *G* and *J*). This indicates that if the kinetic isotope fractionation existed, its role was limited. The observed isotope profiles are still best portraited by the Rayleigh distillation model as shown in Fig. 2. and the estimated α may reflect the combined effect of thermodynamic and secondary kinetic isotope fractionation.

The average α values for all six samples range from 0.99955 to 0.99988 (Fig. 2 and *SI Appendix*, Table S6), covering 0.9995 inferred from Hekla volcanic rocks (21). The obtained values are all below 1, confirming the preference of light Zr isotope in zircon. Moreover, α varies systematically among the hornblende gabbros (0.99974–0.99988), tonalites (0.99974–0.99978), and biotite-rich enclave (0.99955) (Fig. 4*B*). This suggests that the Zr isotope evolution of magmatic systems is a dynamic process and a constant α may not be able to fully describe this process.

Temperature dependence of Zr isotope fractionation

As shown above, the zircon–melt fractionation factor α may vary in magmas of different temperatures and compositions. It is important to assess the potential controlling factor(s) on α. As predicted by classic stable isotope fractionation theories (47), mass-dependent fractionation should have a strong temperature dependence. At high-temperature conditions, the relationship between α for thermodynamic fractionation and the temperature (T, in Kelvin) is described as:

$$1000 \ln(\alpha) = A \times 10^6/T^2 + B \quad (3)$$

Where A and B are equilibrium constants, and B should be 0 since fractionation approaches 0‰ at infinitely high temperatures. This equation is also the theoretical base for stable isotope thermometers. We use the average α value and median Ti-in-zircon temperature of zircon to evaluate the temperature dependence of Zr isotope fractionation (Fig. 4*B*). The temperatures vary from 743–831 °C for hornblende gabbros, 726–742 °C for tonalites, to 689 °C for the biotite-rich enclave (*SI Appendix*, Table S2). The correlation (square of the correlation coefficient, $r^2 = 0.86$) between 1000 ln(α) and $1/T^2$ is obtained as below (Fig. 4*B*):

$$1000 \ln(\alpha) = -0.95\pm0.84 \times 10^6/T^2 + 0.65\pm0.81 \quad (4)$$

The correlation relies on the estimated fractionation factor, and thus the assumed initial melt composition for the modeling. It should be noted that the free term B is not zero, which is probably caused by (1) uncertainties in our data (the sample size is not large enough at present) and in the formula extrapolation; and (2) to a lesser extent, the potential kinetic isotope fractionation as mentioned above (if present). Underestimated α for zircons in low-T samples due to potential kinetic isotope fractionation would cause a steeper slope and a non-zero B in Fig. 4*B*. Additionally, the melt composition may result in changes in Zr bonding environment and thus the α, but its role remains unknown (24). Given the large uncertainty in the regression, this empiric Equation (4) so far cannot be applied to estimate precise temperature, which requires future calibration. Nonetheless, the good correlation ($r^2 = 0.86$) itself still indicates strong temperature dependence of zircon–melt Zr isotope fractionation.

The empirical Equation (4) indicates that α will drop from 0.99983 to 0.99965 when temperatures decrease from 800 °C to 700 °C. At temperatures >850 °C, limited isotope fractionation (<0.1‰) is expected, whereas at lower temperatures, fractionation is expected to be more significant especially for felsic magmas that may reach early zircon saturation. This equation also implies the potential use of simple zircon Zr isotope zoning as a tracer for magma temperatures. After future experimental or theoretical calibrations, it may provide independent temperature constraints on magmatic thermal history. Another application would be the estimation of initial melt composition ($1000 \ln(\alpha) \approx \delta^{94}Zr_{zircon,\ core} - \delta^{94}Zr_{melt,\ 0}$, and it is also noted that the rim composition is generally

close to the assumed initial melt in Fig. 2) if the temperature can be constrained by other thermometers (Fig. 4*B*), which may be applicable to trace magmatic Zr isotope evolution.

Tracing magmatic evolution history and continental crustal differentiation

Our study shows the importance of in-situ zircon Zr isotope analyses in understanding the chemical and thermal evolution of calc-alkaline magmatic systems. These systems have played a major role in producing the continental crust (48). Magmatic zircon can preserve growth zoning of both Zr isotopes (Fig. 2) and trace elements (49) due to its low solubility in crustal melts, high resistance to chemical/physical breakdown, and low diffusivities of trivalent and tetravalent cations (e.g., REE, Zr, Hf, U, and Th) (25, 50). Unlike the trace element zoning that is controlled by multiple factors (such as pressures and temperatures, melt compositions, coexisting minerals, and the growth rate of zircon) (49, 51), the Zr isotope zoning in magmatic zircons is less complex and mainly controlled by the melt composition and temperature (Figs. 4*B* and 5). Technically, it is also much easier to achieve high-spatial resolution and high-precision for laser ablation in-situ Zr isotope as Zr is a major element of zircon with limited isotopic interferences (this study and ref. 15). For zircon grains with simple growth history (Figs. 5 *B* and *D*), their internal Zr isotope profiles can be used to constrain the magma temperature or composition by applying the empirically calibrated correlation between zircon–melt α and the magma temperature. For zircons with relatively complex growth history (e.g., Fig. 5*C*), differences between anatectic cores and autocrystic rims may reveal additional information on the magmatic evolution history. For example, an anatectic core, with a truncation surface in CL images and discontinuously higher (or lower) δ^{94}Zr values, may have formed at higher (or lower) temperatures than the rim (Fig. 5*C*). Together with other zircon-based geochemical tools, stable Zr isotopes would have wide applications in depicting magmatic processes such as magma assimilation and recharge or pre-eruption volcanic processes.

The internal isotope profile of single magmatic zircon further suggests that zircon preferentially incorporate light Zr isotopes, which means that the heavy ones would be concentrated in the residual melt, especially in the late-stage differentiation products of magmas. Zirconium, as an incompatible element during mantle melting and early magma differentiation (17, 18), is favored by the melt that eventually formed the continental crust of the Earth (48). Large fractionation among its isotopes is supposed to occur at late stages when the residual melts evolve to felsic compositions (>65 wt.% SiO_2) by liquid–crystal segregation (18, 21). The oceanic crust has a basaltic composition (SiO_2 ~50 wt.%) and a relatively low Zr content (~70 ppm) (52), and large Zr isotope fractionation is not expected. This is consistent with the observed narrow variation range of δ^{94}Zr (−0.033‰ to 0.086‰) in oceanic basalts (21). In comparison, the continental crust has an average andesitic composition with higher SiO_2 (~60 wt.%) and Zr contents (132 ppm) (48). Thus much larger Zr isotope fractionation is expected in rocks from the continental crust. The upper

continental crust, as an archive of late-stage magmatic products, has a more evolved average composition of 66.6 wt.% SiO_2 and 193 ppm Zr (48), which should be isotopically heavier than the primitive mantle. When the crust becomes more mature, the enrichment degree of heavy Zr isotopes in the upper crust should also increase. Thus, the Zr isotope composition of the upper crust in different continental regions may be used as an indicator for crustal maturation. Once confirmed, zircon Zr isotopes may open a new and insightful way to understand the evolution of the continental crust over geological time (from 4.4 billion years by Jack Hill zircons to present), particularly at the early stage of the first one or two billion years when the geological record but zircon has been relatively rare.

Conclusions

We present new in-situ Zr isotope compositions of magmatic zircon in a calc-alkaline plutonic suite from the juvenile part of the Gangdese arc, southern Tibet. The Zr isotope data were obtained by laser ablation MC-ICP-MS with a high spatial resolution (20 μm) and high precision (2SD <0.15‰ for $\delta^{94}Zr$). The results show large variations ranging from −0.86‰ to 0.41‰, and most individual zircon grains exhibit internal zoning with low $\delta^{94}Zr$ in the core and higher values toward the rim. This indicates that zircon favors light Zr isotopes from the melt, and its crystallization would drive melt to heavier Zr isotope compositions. This would set the base for future interpretation of the Zr isotope evolution in calc-alkaline igneous rocks, the major constituent of the continental crust. The observed isotope profiles in single zircon grains can be well explained by the Rayleigh distillation model. The best fit-models gave different average α values (0.99955–0.99988) for the studied samples, which are positively correlated with the median Ti-in-zircon temperatures, indicating a strong temperature dependence of zircon–melt Zr isotope fractionation. The results also demonstrate that in-situ Zr isotope profiles in zircon could provide key insights into the chemical and thermal history of magmatic systems. The stable Zr isotope is a promising powerful tracer in revealing the differentiation of terrestrial magmatic systems and the Earth's continental crust.

Methods

The stable Zr isotopes of zircon were analyzed by using an NWRfemto femtosecond LA system (New Wave Research, USA) coupled with a Neptune Plus MC-ICP-MS (Thermo Fisher Scientific, Bremen, Germany) at the China University of Geosciences, Wuhan. The spot size was set to 20 μm. The ablation frequency was as low as 1 Hz, which reduced the risk of isotope fractionation induced by small-beam laser ablation. Zircon U–Pb dating and trace element analyses were performed by using a 193 nm excimer ArF LA system (GeoLas HD, Coherent Inc., Göttingen,

Germany) coupled with Agilent 7700x quadrupole ICP-MS. Major and trace element compositions of zircon were further analyzed next to Zr isotope profiles by using GeoLas Pro 193 nm excimer ArF LA system coupled with Agilent 7700e ICP-MS at the Wuhan SampleSolution Analytical Technology Co., Ltd., China. The CL images of zircon were taken to reveal the internal structure of zircon by using Analytical Scanning Electron Microscope (JSM-IT100 InTouchScope™, JEOL Ltd.) connected to a MINICL system (Gatan Inc.). The bulk-rock major and trace element compositions were analyzed by using X-ray fluorescence (XRF) and Agilent 7900 quadrupole ICP-MS, respectively. Analytical details can be found in *SI Appendix*.

Data Availability. All data utilized during this study are included within the *SI Appendix* or may be calculated with parameters included therein.

Acknowledgments

We are grateful to two anonymous reviewers for their constructive suggestions that greatly improved the manuscript. We thank Tao Luo for assistance in the LA-ICP-MS lab. This study was supported by the National Key Research and Development Project of China (No. 2016YFC0600309), the National Natural Science Foundation of China (Nos. 41973024 and 41502049), the 111 Project (No. BP0719022), and the Fundamental Research Funds for the Central Universities (No. CUGL180413). M.D. acknowledges support from US National Science Foundation grant EAR 1725002 and the Romanian Executive Agency for Higher Education, Research, Development and Innovation Funding project PN-III-P4-ID-PCCF-2016-0014.

References

1. E. B. Watson, T. M. Harrison, Zircon saturation revisited: Temperature and composition effects in a variety of crustal magma types. *Earth Planet. Sci. Lett.* **64**, 295–304 (1983).
2. F. Corfu, J. M. Hanchar, P. W. O. Hoskin, P. Kinny, Atlas of zircon textures. *Rev. Mineral. Geochem.* **53**, 469–500 (2003).
3. C. Balica, *et al.*, A zircon petrochronologic view on granitoids and continental evolution. *Earth Planet. Sci. Lett.* **531**, 116005 (2020).
4. T. M. Harrison, The Hadean crust: Evidence from >4 Ga zircons. *Annu. Rev. Earth Planet. Sci.* **37**, 479–505 (2009).
5. T. M. Harrison, E. A. Bell, P. Boehnke, Hadean zircon petrochronology. *Rev. Mineral. Geochem.* **83**, 329–363 (2017).
6. D. Rubatto, Zircon trace element geochemistry: Partitioning with garnet and the link between U–Pb ages and metamorphism. *Chem. Geol.* **184**, 123–138 (2002).
7. D. Trail, *et al.*, Origin and significance of Si and O isotope heterogeneities in Phanerozoic, Archean, and Hadean zircon. *Proc. Natl. Acad. Sci. U. S. A.* **115**, 10287–10292 (2018).
8. J. W. Valley, Oxygen isotopes in zircon. *Rev. Mineral. Geochem.* **53**, 343–385 (2003).
9. C. J. Hawkesworth, A. I. S. Kemp, Using hafnium and oxygen isotopes in zircons to unravel the record of crustal evolution. *Chem. Geol.* **226**, 144–162 (2006).
10. A. I. S. Kemp, *et al.*, Hadean crustal evolution revisited: New constraints from Pb–Hf isotope systematics of the Jack Hills zircons. *Earth Planet. Sci. Lett.* **296**, 45–56 (2010).
11. M. Hopkins, T. M. Harrison, C. E. Manning, Low heat flow inferred from >4 Gyr zircons suggests Hadean plate boundary interactions. *Nature* **456**, 493–496 (2008).
12. N. M. W. Roberts, C. J. Spencer, The zircon archive of continent formation through time. *Geol. Soc. Spec. Publ.* **389**, 197–225 (2015).
13. D. J. Cherniak, E. B. Watson, Diffusion in Zircon. *Rev. Mineral. Geochem.* **53**, 113–143 (2003).
14. T. M. Harrison, A. K. Schmitt, High sensitivity mapping of Ti distributions in Hadean zircons. *Earth Planet. Sci. Lett.* **261**, 9–19 (2007).
15. W. Zhang, *et al.*, Determination of Zr isotopic ratios in zircons using laser-ablation multiple-collector inductively coupled-plasma mass-spectrometry. *J. Anal. At. Spectrom.* **34**, 1800–1809 (2019).
16. F. Bea, P. Montero, M. Ortega, A LA–ICP–MS evaluation of Zr reservoirs in common crustal rocks: Implications for Zr and Hf geochemistry, and zircon-forming processes. *Can. Mineral.* **44**, 693–714 (2006).
17. A. W. Hofmann, Chemical differentiation of the Earth: The relationship between mantle, continental crust, and oceanic crust. *Earth Planet. Sci. Lett.* **90**, 297–314 (1988).
18. C.-T. A. Lee, O. Bachmann, How important is the role of crystal fractionation in making intermediate magmas? Insights from Zr and P systematics. *Earth Planet. Sci. Lett.* **393**, 266–274 (2014).
19. W. Akram, M. Schönbächler, Zirconium isotope constraints on the composition of Theia and current Moon-forming theories. *Earth Planet. Sci. Lett.* **449**, 302–310 (2016).
20. E. C. Inglis, J. B. Creech, Z. Deng, F. Moynier, High-precision zirconium stable isotope measurements of geological reference materials as measured by double-spike MC-ICPMS. *Chem. Geol.* **493**, 544–552 (2018).

21. E. C. Inglis, *et al.*, Isotopic fractionation of zirconium during magmatic differentiation and the stable isotope composition of the silicate Earth. *Geochim. Cosmochim. Acta* **250**, 311–323 (2019).

22. M. Ibañez-Mejia, F. L. H. Tissot, Extreme Zr stable isotope fractionation during magmatic fractional crystallization. *Sci. Adv.* **5**, eaax8648 (2019).

23. L. Feng, *et al.*, High-precision stable zirconium isotope ratio measurements by double spike thermal ionization mass spectrometry. *J. Anal. At. Spectrom.* **35**, 736–745 (2020).

24. H. G. D. Tompkins, L. J. Zieman, M. Ibañez-Mejia, F. L. H. Tissot, Zirconium stable isotope analysis of zircon by MC-ICP-MS: Methods and application to evaluating intra-crystalline zonation in a zircon megacryst. *J. Anal. At. Spectrom.* **35**, 1167–1186 (2020).

25. D. J. Cherniak, J. M. Hanchar, E. B. Watson, Diffusion of tetravalent cations in zircon. *Contrib. Mineral. Petrol.* **127**, 383–390 (1997).

26. W.-Q. Ji, F.-Y. Wu, S.-L. Chung, J.-X. Li, C.-Z. Liu, Zircon U–Pb geochronology and Hf isotopic constraints on petrogenesis of the Gangdese batholith, southern Tibet. *Chem. Geol.* **262**, 229–245 (2009).

27. W.-C. Xu, H.-F. Zhang, B.-J. Luo, L. Guo, H. Yang, Adakite-like geochemical signature produced by amphibole-dominated fractionation of arc magmas: An example from the Late Cretaceous magmatism in Gangdese belt, south Tibet. *Lithos* **232**, 197–210 (2015).

28. A. Yin, T. M. Harrison, Geologic evolution of the Himalayan-Tibetan orogen. *Annu. Rev. Earth Planet. Sci.* **28**, 211–280 (2000).

29. S. E. Jackson, N. J. Pearson, W. L. Griffin, E. A. Belousova, The application of laser ablation-inductively coupled plasma-mass spectrometry to in situ U–Pb zircon geochronology. *Chem. Geol.* **211**, 47–69 (2004).

30. X. H. Li, *et al.*, Penglai zircon megacrysts: A potential new working reference material for microbeam determination of Hf–O isotopes and U–Pb age. *Geostand. Geoanal. Res.* (2010).

31. C. Siégel, S. E. Bryan, C. M. Allen, D. A. Gust, Use and abuse of zircon-based thermometers: A critical review and a recommended approach to identify antecrystic zircons. *Earth-Sci. Rev.* **176**, 87–116 (2018).

32. L. L. Claiborne, *et al.*, Tracking magmatic processes through Zr/Hf ratios in rocks and Hf and Ti zoning in zircons: An example from the Spirit Mountain batholith, Nevada. *Mineral. Mag.* **70**, 517–543 (2006).

33. J. M. Ferry, E. B. Watson, New thermodynamic models and revised calibrations for the Ti-in-zircon and Zr-in-rutile thermometers. *Contrib. Mineral. Petrol.* **154**, 429–437 (2007).

34. D. Schiller, F. Finger, Application of Ti-in-zircon thermometry to granite studies: Problems and possible solutions. *Contrib. Mineral. Petrol.* **174**, 51 (2019).

35. J. A. D. Connolly, K. Petrini, An automated strategy for calculation of phase diagram sections and retrieval of rock properties as a function of physical conditions. *J. Metamorph. Geol.* **20**, 697–708 (2002).

36. F. Farges, The structure of metamict zircon: A temperature-dependent EXAFS study. *Phys. Chem. Miner.* **20**, 504–514 (1994).

37. F. Farges, C. W. Ponader, G. E. Brown, Structural environments of incompatible elements in silicate glass/melt systems: I. Zirconium at trace levels. *Geochim. Cosmochim. Acta* **55**, 1563–1574 (1991).

38. T. Tobase, *et al.*, XAFS study on the Zr local structures in tektites and natural glasses. *J. Miner. Petrol. Sci.* **110**, 1–7 (2015).

39. M. Takehara, K. Horie, T. Hokada, S. Kiyokawa, New insight into disturbance of U-Pb and trace-element systems in hydrothermally altered zircon via SHRIMP analyses of zircon from the Duluth Gabbro. *Chem. Geol.* **484**, 168–178 (2018).

40. D. Frei, A. Gerdes, Precise and accurate in situ U–Pb dating of zircon with high sample throughput by automated LA-SF-ICP-MS. *Chem. Geol.* **261**, 261–270 (2009).

41. I. N. Bindeman, O. E. Melnik, Zircon survival, rebirth and recycling during crustal melting, magma crystallization, and mixing based on numerical modelling. *J. Petrol.* (2016).

42. T. M. Harrison, E. B. Watson, Kinetics of zircon dissolution and zirconium diffusion in granitic melts of variable water content. *Contrib. Mineral. Petrol.* **84**, 66–72 (1983).

43. M. E. Holycross, E. B. Watson, Trace element diffusion and kinetic fractionation in wet rhyolitic melt. *Geochim. Cosmochim. Acta* **232**, 14–29 (2018).

44. E. B. Watson, T. Müller, Non-equilibrium isotopic and elemental fractionation during diffusion-controlled crystal growth under static and dynamic conditions. *Chem. Geol.* **267**, 111–124 (2009).

45. E. B. Watson, Surface enrichment and trace-element uptake during crystal growth. *Geochimica et Cosmochimica Acta* **60**, 5013–5020 (1996).

46. A. K. Schmitt, *et al.*, Acigöl rhyolite field, Central Anatolia (part 1): High-resolution dating of eruption episodes and zircon growth rates. *Contrib. Mineral. Petrol.* **162**, 1215–1231 (2011).

47. H. C. Urey, The thermodynamic properties of isotopic substances. *J. Chem. Soc.*, 562–581 (1947).

48. R. L. Rudnick, S. Gao, “4.1 - Composition of the Continental Crust” in *Treatise on Geochemistry (Second Edition)*, H. D. Holland, K. K. Turekian, Eds. (Elsevier, 2014), pp. 1–51.

49. P. W. O. Hoskin, Patterns of chaos: Fractal statistics and the oscillatory chemistry of zircon. *Geochim. Cosmochim. Acta* **64**, 1905–1923 (2000).

50. D. J. Cherniak, Si diffusion in zircon. *Phys. Chem. Miner.* **35**, 179–187 (2008).

51. O. E. Melnik, I. N. Bindeman, Modeling of trace elemental zoning patterns in accessory minerals with emphasis on the origin of micrometer-scale oscillatory zoning in zircon. *Am. Mineral.* **103**, 355–368 (2018).

52. S. S. Sun, W. F. McDonough, Chemical and isotopic systematics of oceanic basalts: Implications for mantle composition and processes. *Geol. Soc. Spec. Publ.* **42**, 313–345 (1989).

Figures legends

Fig. 1. Scanned images of thick petrographic sections for plutonic rocks from the Gangdese arc, southern Tibet. (*A*–*C*) Hornblende gabbros. (*D*–*E*) Tonalites. (F) Biotite-rich enclave. Hb = hornblende, Bi = biotite.

Fig. 2. Representative Zr isotope and Zr/Hf profiles of magmatic zircon in plutonic rocks from the Gangdese arc, southern Tibet. (*A*–*F*) Hornblende gabbros. (*G*–*J*) Tonalites. (*K*–*L*) Biotite-rich enclave. Blue curves denote best-fit isotope profiles modeled from the Rayleigh distillation equation. Dotted grey lines indicate the initial melt composition used for modeling. Corresponding cathodoluminescence images of zircon are presented on the left, showing the internal structures. Solid yellow, dotted red, and dashed white circles denote laser ablation spots for Zr isotopes (20 μm in diameter), Zr/Hf profiles (24 μm in diameter), and U–Pb isotopes and trace elements (32 μm in diameter), respectively. Error bars for the δ^{94}Zr and Zr/Hf ratios represent ±2SE uncertainties.

Fig. 3. Intragrain core-to-rim Zr isotope variations in zircon from plutonic rocks in the Gangdese arc, southern Tibet. (*A*) Three representative zircon grains for each sample. (*B*–*G*) Histograms of δ^{94}Zr values for the core, mantle, and rim of all zircon grains in each sample. N is the number of total analyses for each sample. Dotted red lines denote the primitive mantle value of 0.048±0.032‰ (2SD) (21). Error bars represent ±2SE uncertainty. Hb = hornblende, Bi = biotite.

Fig. 4. The fractionation mechanism of Zr isotopes between zircon and melt. (*A*) Rayleigh distillation modeling of Zr isotope evolution of crystallizing zircons and the residual melts. Solid and dashed lines denote the zircon and the melt, respectively. The initial melt composition was assumed to be 0.05‰. (*B*) Correlation between average fractionation factor α and median Ti-in-zircon temperatures (T) for the studied samples. Fractionation factors were estimated from the best-fit Rayleigh distillation models. The overall trend indicates a strong temperature dependence, but large uncertainty exists in the regression and cautions are needed when applying the obtained empiric equation. Error bars represent ±2SE uncertainty. The shaded area indicates the 95% confidence interval.

Fig. 5. Schematic of zircon-induced Zr isotope fractionation during magma differentiation and examples of the produced Zr isotope profiles in single zircon grain, showing the potential of Zr isotopes in tracing the differentiation of magmatic systems and the continental crust. The isotope profiles in zircon were modeled from the Rayleigh distillation equation, assuming an initial melt composition of 0.05‰ (dotted grey lines) with fractionation factor α calculated from Equation (4)

at given temperatures. (*A*) Light Zr isotopes in calc-alkaline magmas are preferentially incorporated by zircon, driving the residual melt to isotopically heavier compositions. Due to the strong temperature (T) dependence of zircon–melt Zr isotope fractionation, larger isotope fractionation is expected when magmas evolve to lower temperatures. (*B*) Modeled Zr isotope profile in zircon crystallized at 700 °C with a simple growth history. (*C*) Modeled Zr isotope profile in zircon with a complex growth history. The rim (solid blue line) and the core (dashed orange line) were calculated at temperatures of 700 °C and 800 °C, respectively. Note that complex zoning patterns may exist in natural zircons. (*D*) Modeled Zr isotope profile of zircon crystallized at 800 °C with a simple growth history.

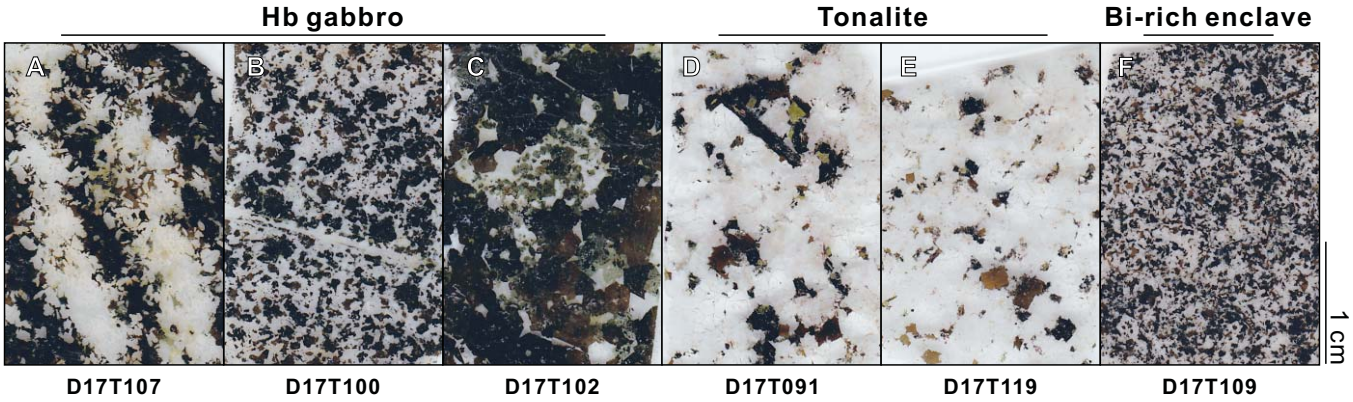
Hb gabbro
Tonalite
Bi-rich enclave
A
B
C
D
E
F
1 cm
D17T107
D17T100
D17T102
D17T091
D17T119
D17T109

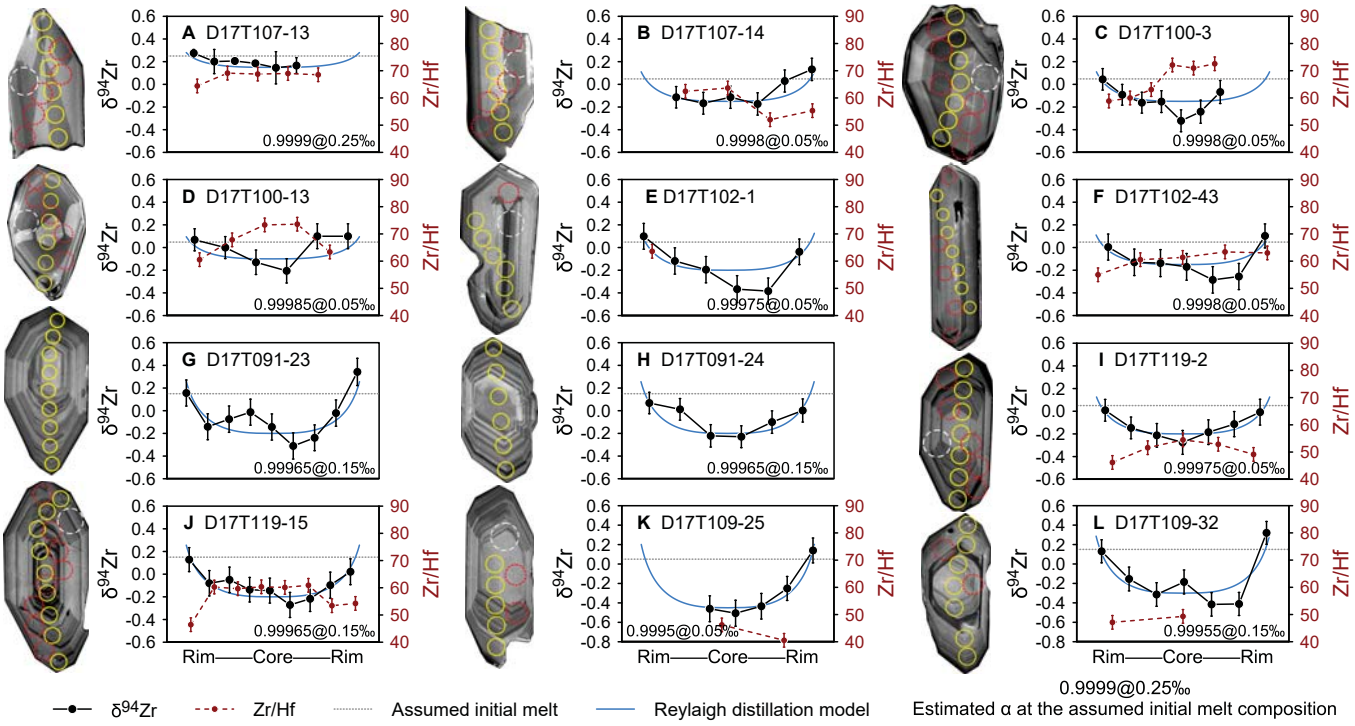
A D17T107-13
0.9999@0.25‰
B D17T107-14
0.9998@0.05‰
C D17T100-3
0.9998@0.05‰
D D17T100-13
0.99985@0.05‰
E D17T102-1
0.99975@0.05‰
F D17T102-43
0.9998@0.05‰
G D17T091-23
0.99965@0.15‰
H D17T091-24
0.99965@0.15‰
I D17T119-2
0.99975@0.05‰
J D17T119-15
0.99965@0.15‰
K D17T109-25
0.9995@0.05‰
L D17T109-32
0.99955@0.15‰
δ94Zr
Zr/Hf
Rim——Core——Rim
δ94Zr
Zr/Hf
Assumed initial melt
Reylaigh distillation model
0.9999@0.25‰
Estimated α at the assumed initial melt composition

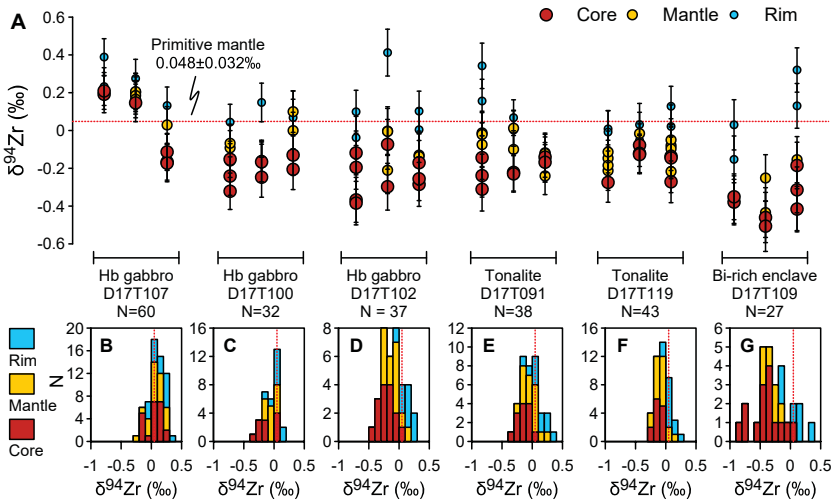
A
Core
Mantle
Rim
Primitive mantle
0.048±0.032‰
δ94Zr (‰)
Hb gabbro
D17T107
N=60
Hb gabbro
D17T100
N=32
Hb gabbro
D17T102
N = 37
Tonalite
D17T091
N=38
Tonalite
D17T119
N=43
Bi-rich enclave
D17T109
N=27
Rim
Mantle
Core
N
B
C
D
E
F
G
δ94Zr (‰)

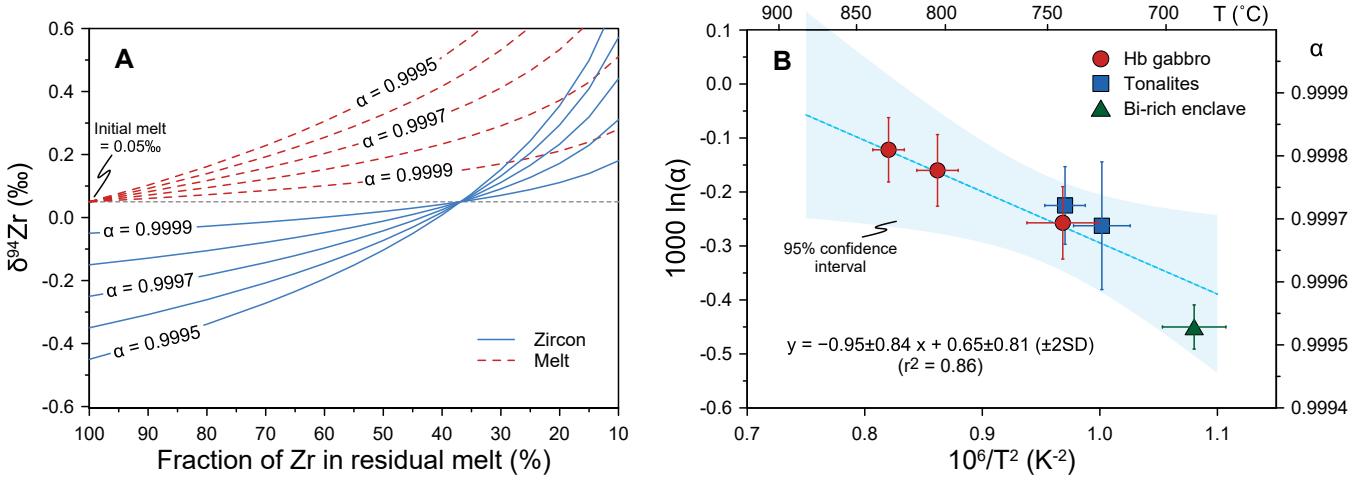
A
Initial melt
= 0.05‰
α = 0.9995
α = 0.9997
α = 0.9999
α = 0.9999
α = 0.9997
α = 0.9995
Zircon
Melt
δ94Zr (‰)
Fraction of Zr in residual melt (%)
B
Hb gabbro
Tonalites
Bi-rich enclave
95% confidence
interval
y = −0.95±0.84 x + 0.65±0.81 (±2SD)
(r2 = 0.86)
1000 ln(α)
T (˚C)
α
10⁶/T² (K⁻²)

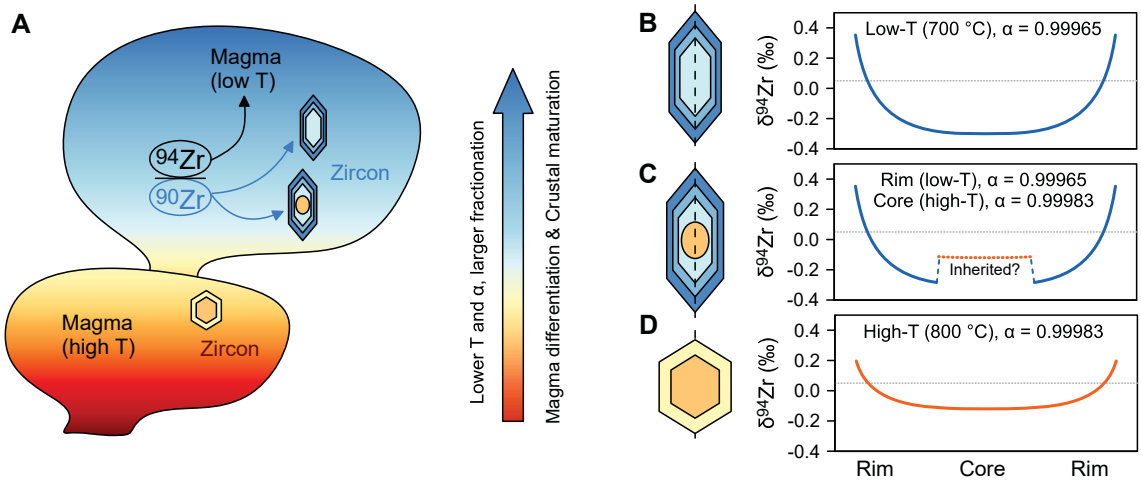
A
Magma
(low T)
94Zr
90Zr
Zircon
Magma
(high T)
Zircon
Lower T and α, larger fractionation
Magma differentiation & Crustal maturation
B
C
D
Low-T (700 °C), α = 0.99965
Rim (low-T), α = 0.99965
Core (high-T), α = 0.99983
Inherited?
High-T (800 °C), α = 0.99983
δ94Zr (‰)
0.4
0.2
0.0
-0.2
-0.4
Rim
Core
Rim